Virtual Reconstruction of Archaeological Vessels using Expert Priors & Surface Markings

Fernand Cohen*, Ezgi Taslidere*, Zexi Liu*, and Glen Muschio**
*Electrical and Computer Engineering Department, ** Digital Media Program
Drexel University
Philadelphia, PA 19104
fscohen@coe.drexel.edu

Abstract

This paper presents a method to assist in the tedious procedure of reconstructing ceramic vessels from unearthed archaeological shards or fragments using 3D computer vision-enabling technologies. The method uses vessels surface markings combined with a generic model to produce a representation of what the original vessel may have looked like. .Generic vessel models used are based on a host of factors including expert historical knowledge of the period, provenance of the artifact and site location. The generic model need not be identical to the excavated vessel, but must be within the allowable class, i.e., it is within a geometric transformation of it in most of its parts. The ceramic vessels we worked with have markings, which we exploit under the allowable set of transformations between the generic model and the excavated vessel. We align them using a novel set of weighted curve moments. The morphing transformation (affine or higher order morphing function) is computed from these corresponding curves, and distance error metrics are introduced to access the accuracy of alignment of a fragment to a given vessel. If a vessel has no surface markings, we use curves for alignment these are computed from the intrinsic differential geometry of the surface and are also locally affine preserved. The methods are tested on a subset of Independence National Historical Park (INDE) ceramic artifacts created by 3-D scanning of prospective generic bowls and their pieces.

1. Introduction

The analysis of unearthed archeological ceramic shards to reconstruct vessels that the fragments once formed is currently a tedious and time-consuming process. Nevertheless, it is a vital step in interpreting the archaeological record and an important component in understanding and preserving cultural heritage. 3D computer vision-enabling technologies have the potential to automate at least part of the traditional reconstruction process [1-9] and offer the promise of transforming the entire archaeological journey from *primary evidence collecting* to *public history interpretation*. The use of cost effective and efficient computer technologies for reconstruction tasks are currently being modeled and tested using 18th century archaeological data - specifically ceramic shards and vessels - excavated from a site in Independence National Historical Park in Philadelphia, Pennsylvania (Figure 1).

There are a variety of existing techniques for reconstructing fragments using computer vision technology [10-17]. The unifying idea rests on finding corresponding parts, matching them, aligning them and gluing all matching parts together [18]. Accordingly, there are three basic matching primitives in 3D; point-by-point, curve and surface matching. In the literature reviewed, most of the existing approaches take a "boundary matching" approach. This method makes use of matching the boundaries of associated pieces. When dealing with archaeological ceramic artifacts that have been in the ground for many years, the edges of the sherds may suffer from erosion. This can make matching the boundaries of associated sherds difficult. To avoid the difficulty, we have selected a surface-based approach rather than a boundary matching approach. Surface information including surface markings is generally better preserved than fragment boundaries. Furthermore, the surface of a 3D object carries valuable information useful in characterizing the object. The surface base approach is not without its problems, concerns include the difficulty of data acquisition and organizing the data after acquisition.

In this paper, we develop methods that make use of expertly derived generic vessel models to drive the alignment of artifacts against these vessels. As the generic vessel model is not exact, but produced through approximations to the excavated vessels, our alignment method allows for model uncertainties and seeks robust local fiducial points or features to drive the alignment. We present a novel approach to exploiting the surface markings, which extracts the contours of the markings and models them as B-Spline 3D curves [19-21]. The B-Spline curve model is locally affine preserved, i.e., it carries through and up to a local affine map, i.e., it carries to nonlinear maps that are piecewise affine. The markings models are robust to a host of allowable transformations between the vessel and the generic model as to be able to take care of small variations (rotation, scaling, translation, compression, etc) within each classification as well as to parts that are not accounted for by the allowable

978-1-4244-7028-0/10/$26.00 ©2010 IEEE

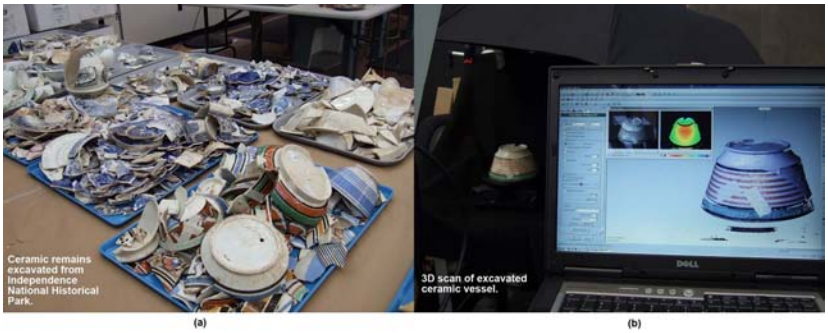

Figure 1: Ceramic Remains.

transformations. Moreover, it is local, which means that a part will still be correctly aligned even when some small part of it is not accounted for by the generic model and the transformation. Corresponding curve markings are established using weighted moments computed from the B-Spline curves. The novel moments also carry through the local affine map. Corresponding curve markings are established using absolute affine invariants derived from these weighted moments. We also briefly extend the approach for vessels that have no markings on their surfaces. In this case, the curves that we use for the alignment are computed from the intrinsic differential geometry of the surface and are also local affine preserved. The morphing transformation (affine or higher order morphing function) is computed from these corresponding curves, and distance error metrics are introduced to access the accuracy of alignment of a fragment to a given vessel. These methods are illustrated using ceramic artifact collection recovered from the National Constitution Center site [22].

This paper is organized as follows. Archaeological motivation for our 3-D surface modeling and analysis is presented in Section 2. The details of our data collection process are given in Section 3. In the rest of the paper, two different surface alignment approaches for possible aspects of data are presented and their performances are investigated. Section 4 presents the details of extraction of surface markings and B-Spline curve representations on them. Section 5 gives the details of surface alignment using novel weighted moment invariants on extracted surface marking contours and the results based on that. In Section 6, we discuss a case where the artifacts do not have enough surface texture information and for these cases we introduce B-Spline surface representation, extraction of parabolic contours / fiducial points, and we report the corresponding results. Finally, conclusions and future directions are given in Section 7.

2. Archeological Motivation

Our 3-D surface modeling and feature extraction research is motivated by the necessity of reconstruction of unearthed archeological pieces to discover, preserve, and interpret history. The focus of the project is on ceramic and other artifacts from one of the best preserved and most diverse American urban colonial archaeological sites ever excavated - the Mall at Independence National Historical Park (INDE) in Philadelphia, Pennsylvania [23]. This project is seen by INDE archeologists as having a great potential to have significant implications for archeological artifact mending, collections management, and site interpretation [22]. Once operational on a full scale, this technology will allow for more efficient laboratory work and will produce a significant time and money savings. Computers (not just people) will be able to match up the decorative markings on, and the shapes of, ceramic fragments so as to 'piece back together' broken vessels. Such vessel reconstruction is a vital first step in the laboratory processing of artifacts. Speeding up this phase means faster advancement to the analysis phase of study (as artifact identification precedes site analysis). Computer-assisted vessel reconstructions will furthermore allow for remote research capabilities as a collection of ceramics will be able to be studied off-site via digital proxies. Moreover, the digital images created during the reconstruction process will be a useful resource for virtual history presentations. Records from this research and development project will be archived as part of the INDE Archaeological Records Collection.

3. Data Collection

The ceramic artifact collection recovered from the National Constitution Center site is used as a data set in this project [22]. The artifact collection is currently kept at Independence Living History Center in Philadelphia, PA. Some of the artifacts are mended by the experts by either using glue or bands. Suitable samples of that artifact collection are chosen as to serve as generic models and test samples. The chosen ceramic vessels are scanned at Independence Living History Center Archeology Lab, Philadelphia, PA using a Konica Minolta Vivid 910 3D scanner [24]. Konica Minolta describes the VIVID 910 3D scanner as employing laser-beam light sectioning technology to scan pieces using a split beam; light reflected from the piece is acquired by a CCD camera, and

3D data is then created by triangulation to determine distance information [24]. The scanning is performed using the software tool Geomagic Studio [25] and the scans[1] are processed there to obtain the raw data for the programs. The data set includes 3 different bowls with the names/numbers given by the expert/archeologist as: 1. F191C105, 2. F193C112, 3. F193C0122. Each bowl is put together by the expert from the unearthed pieces. After the whole bowls are scanned, the constructed pieces are taken apart by the expert and those individual pieces are scanned one by one. A sample picture taken during the scanning process is shown in Figure 2.

Figure 2: Sample picture taken during scanning of the pieces of a pedestal saucer.

4. Extracting the Vessel Marking Contours and B-Spline Curve Representation

The marking contours on the vessels are extracted using thresholding the color information of the scanned 3D texture. After extracting all the surface contours, each surface contour can be represented as a 3-D B-Spline space curve given as [21]:

$$r(u) = \sum_{j=0}^{l} C_j N_{j,p}(u) \qquad (1)$$

$N_{i,p}(u)$ is the basis B-Spline function and given by [26]:

$$N_{i,p}(u) = \frac{u-u_i}{u_{i+p}-u_i} N_{i,p-1}(u) + \frac{u_{i+p+1}-u}{u_{i+p+1}-u_{i+1}} N_{i+1,p-1}(u) \quad ,$$

$$N_{i,0}(u) = \begin{cases} 1 & u_i \le u \le u_{i+1} \\ 0 & elsewhere \end{cases} \qquad (2)$$

where U is the knot vector in u direction, $U = \{u_0, u_1, ..., u_m\}$. The u parametrization is done using Inverse Chord Length (ICL) method: ICL method assigns u_k by making the time taken in traveling between any consecutive points inversely proportional to the chord length between them [19, 27].

[1] Freshman Girish Balakrishnan and David Myers assisted with the scanning. Both are students in Drexel's Honor College program Students Tracking Advanced Research (STAR).

5. Reconstruction of Pieces/Surface Alignment using Moment Invariants on Surface Contours

5.1. Affine-Invariant 3-D Moments for B-Spline Curve Matching

3D moments are defined in terms of the Riemann integral as:

$$m(p,q,r) = \iiint_R x^p y^q z^r f(x,y,z)dxdydz \qquad (3)$$

Volume moments can be used for representing shapes of 3D objects. For the moments to be of use they need to be tractable before and after the affine map and since the information that we have about the 3D is embedded in the marking contours, we also need to use contour integration to compute these moments. To achieve that we introduce a novel set of weighted moments computed from the 3D curve, where the weight kernel factor out the dependency on the affine parameter linearly. One such kernel will be based on volume information which is a relative affine invariant under the affine map. Under an affine transformation $\mathbf{T} = \{[\mathbf{L}], \mathbf{b}\}$ where

$$[\mathbf{L}] = \begin{bmatrix} a_{11} & a_{12} & a_{13} \\ a_{21} & a_{22} & a_{23} \\ a_{31} & a_{32} & a_{33} \end{bmatrix} \quad , \quad \mathbf{b} = \begin{bmatrix} b_1 \\ b_2 \\ b_3 \end{bmatrix} \qquad (4)$$

volume is preserved (is a relative invariant) given as $\tilde{V} = \det\{[\mathbf{L}]\}V$.

A B-Spline curve subjected to affine transformation is still a B-Spline curve where its control points are also subjected to same affine transformation. The transformed B-Spline curve ($\tilde{r}(\tilde{s})$) will be related to the original curve ($r(s)$) through the following equation where affine transform parameters are defined in Equation 4:

$$\tilde{r}(\tilde{s}) = [\mathbf{L}]r(s) + \mathbf{b} \qquad (5)$$

where $r(s) = [x(s), y(s), z(s)]$ & $\tilde{r}(\tilde{s}) = [\tilde{x}(\tilde{s}), \tilde{y}(\tilde{s}), \tilde{z}(\tilde{s})]$ are the curves before and after the affine map parameterized in terms of arc lengths $s \in [0, S]$ and $\tilde{s} \in [0, \tilde{S}]$, respectively. Their derivative curves will also be linearly related through the same equation as given above (with $\mathbf{b} = 0$). General equation for moments weighted by the j^{th} kind kernel $w_j(x,y,z)$ of a curve $R(s)$

$$ma(p,q,r)^{(j)} = \int_S x^p(s) y^q(s) z^r(s) w_j(x,y,z) ds \qquad (6)$$

The weighting kernels can not be chosen as unity as the parameterization in terms of arc length suffers from the problem that it transforms nonlinearly under the affine transformation [27]. To overcome that problem we use volume as a weighing kernel to factor out the dependency

on affine transform parameters. When there is no translation (when $\mathbf{b}=0$), we define $w_1(x,y,z)$ as:

$$w_1(x,y,z)=\sqrt[3]{\left((x.\frac{dy}{ds}-y.\frac{dx}{ds})\frac{d^2z}{ds^2}\right)+\left((y.\frac{dz}{ds}-z.\frac{dy}{ds})\frac{d^2x}{ds^2}\right)+\left((z.\frac{dx}{ds}-x.\frac{dz}{ds})\frac{d^2y}{ds^2}\right)} \quad (7)$$

The reason for the cubic root in the above equations is to make the exponent of ds's be 1. We know that the differential volume equation is:

$$dV=\frac{1}{6}\det\left\{\begin{bmatrix}x & dx & d^2x\\ y & dy & d^2y\\ z & dz & d^2z\end{bmatrix}\right\}$$

$$=\frac{1}{6}\left\{\left[(x.dy-y.dx)d^2z\right]+\left[(y.dz-z.dy)d^2x\right]+\left[(z.dx-x.dz)d^2y\right]\right\}$$

Hence, $w_1(x,y,z)ds$ in weighted moment equation (equation 6) can be written as written as:

$$w_1(x,y,z)ds=\sqrt[3]{6}\sqrt[3]{dV} \quad (8)$$

Taking the derivative and then cubic root of the volume preservation equation, we have

$$\sqrt[3]{d\tilde{V}}=\sqrt[3]{\det\{[\mathbf{L}]\}}\sqrt[3]{dV} \quad (9)$$

then

$$w_1(\tilde{x},\tilde{y},\tilde{z})d\tilde{s}=\sqrt[3]{\det\{[\mathbf{L}]\}}w_1(x,y,z)ds \quad (10)$$

When there is translation (where $\mathbf{b}\neq 0$), we need to find the derivative curves and construct weights on them. This induces second kind kernel expression ($w_2(x,y,z)$:

$$w_2(x,y,z)=\sqrt[6]{\left((\frac{dx}{ds}.\frac{d^2y}{ds^2}-\frac{dy}{ds}.\frac{d^2x}{ds^2})\frac{d^3z}{ds^3}\right)+\left((\frac{dy}{ds}.\frac{d^2z}{ds^2}-\frac{dz}{ds}.\frac{d^2y}{ds^2})\frac{d^3x}{ds^3}\right)+\left((\frac{dz}{ds}.\frac{d^2x}{ds^2}-\frac{dx}{ds}.\frac{d^2z}{ds^2})\frac{d^3y}{ds^3}\right)} \quad (11)$$

Similarly as in $w_1(x,y,z)$, the reason for the sixth order root in the above equations is to make the exponent of ds's be 1. This time second kernel expressions lead to the differential volume invariance but now applied to the derivative curves ($dr(t)/dt$ and $d\tilde{r}(t)/dt$). General differential volume equation on derivative curve is given as

$$dV_2=\frac{1}{6}\det\left\{\begin{bmatrix}dx & d^2x & d^3x\\ dy & d^2y & d^3y\\ dz & d^2z & d^3z\end{bmatrix}\right\}$$

$$=\frac{1}{6}\left\{\left[(dx.d^2y-dy.d^2x)d^3z\right]+\left[(dy.d^2z-dz.d^2y)d^3x\right]+\left[(dz.d^2x-dx.d^2z)d^3y\right]\right\}$$

Hence $w_2(x,y,z)ds$ in weighted moment equation (equation 6) can be written as:

$$w_2(x,y,z)ds=\sqrt[6]{6}\sqrt[6]{dV_2} \quad (12)$$

Taking the derivative and then sixth order root of the volume preservation equation, we have

$$\sqrt[6]{d\tilde{V}}=\sqrt[6]{\det\{[\mathbf{L}]\}}\sqrt[6]{dV} \quad (13)$$

then

$$w_2(\tilde{x},\tilde{y},\tilde{z})d\tilde{s}=\sqrt[6]{\det\{[\mathbf{L}]\}}w_2(x,y,z)ds \quad (14)$$

Similarly, the 3rd order, 4th order, …, k th kind kernel expressions can be found using 2nd order derivative curve, 3rd order derivative curve, …, (k-1)th order derivative curve, and finally the general expression is given as:

$$w_j(x,y,z)=\sqrt[3j]{\left((\frac{d^{j-1}x}{ds^{j-1}}.\frac{d^jy}{ds^j}-\frac{d^{j-1}y}{ds^{j-1}}.\frac{d^jx}{ds^j})\frac{d^{j+1}z}{ds^{j+1}}\right)+\left((\frac{d^{j-1}y}{d^{j-1}s}.\frac{d^jz}{ds^j}-\frac{d^{j-1}z}{ds^{j-1}}.\frac{d^jy}{ds^j})\frac{d^{j+1}x}{ds^{j+1}}\right)+\left((\frac{d^{j-1}z}{ds^{j-1}}.\frac{d^jx}{ds^j}-\frac{d^{j-1}x}{ds^{j-1}}.\frac{d^jz}{ds^j})\frac{d^{j+1}y}{ds^{j+1}}\right)}$$

$$j=1,2,3,\ldots,k \quad (15)$$

where the B-Spline curve is (k+2)th order and hence C^k-continuous which means its derivatives are continuous up to the k th order.

In order to deal with translation, we calculate the second kernel centroid ($l=2$) for which the general form is:

$$CO^{(l)}=\left(\frac{ma(1,0,0)^{(l)}}{ma(0,0,0)^{(l)}},\frac{ma(0,1,0)^{(l)}}{ma(0,0,0)^{(l)}},\frac{ma(0,0,1)^{(l)}}{ma(0,0,0)^{(l)}}\right) \quad (16)$$

After translating the curves with respect to their own centroids, the translated surfaces are now related through $\mathbf{T}=\{[\mathbf{L}],\mathbf{b}\}$ (where $\mathbf{b}=0$). Then we fit a B-Spline curve to each translated curve $\{(R(s)-CO^{(2)})$ and $(\tilde{R}(s)-\tilde{C}\tilde{O}^{(2)})\}$ and calculate first, third and fourth kernel weighted moments. The transformation parameters of the curves are estimated using the relationship of first, third, and fourth kernel centroids between the curves: $\left[\tilde{C}\tilde{O}^{(1)T}\quad \tilde{C}\tilde{O}^{(3)T}\quad \tilde{C}\tilde{O}^{(4)T}\right]^T=L*\left[CO^{(1)T}\quad CO^{(3)T}\quad CO^{(4)T}\right]^T$ (17)

After estimating $[\mathbf{L}]$, the estimation of $\mathbf{b}$ follows as:

$$\mathbf{b}=\tilde{C}\tilde{O}^{(2)}-[\mathbf{L}]*CO^{(2)} \quad (18)$$

Here the order of the B-Spline should be 7 (degree=6) in order to calculate up to fourth kernel weighted moments.

5.2. Alignment of B-Spline Curves - Surface Contours

The contours on one surface are matched to contours on the other surface one-by-one. For a surface (the artifact piece) having N contours, we pick one of the marking contours, say contour k. Then we try to find the matching contour on the other surface (the generic vessel) using absolute invariants computed from the weighted moment functions and declare a match if the following inequality is satisfied for a pre-specified error percentage (e.g. 0.05)

$$I=\frac{|A-B|}{B}<0.05 \quad (19)$$

A and B are given in terms of the weighted moments as:

$$A=\frac{\left[\tilde{m}\tilde{a}(0,0,0)^{(j)}\right]^{3j}}{\left[\tilde{m}\tilde{a}(0,0,0)^{(i)}\right]^{3i}}\quad,\quad B=\frac{\left[ma(0,0,0)^{(j)}\right]^{3j}}{\left[ma(0,0,0)^{(i)}\right]^{3i}} \quad (20)$$

Once the matching contours are found the estimation of the transformation is done as described in Section 5.1.

The described method is tested on 3 different vessels (1. F191C105, 2. F193C112, 3. F193C0122) which have surface markings on them. One sample piece is chosen for each vessel to be aligned on the generic. The 3D scans of the whole bowls and the pieces are given in Figure 3.

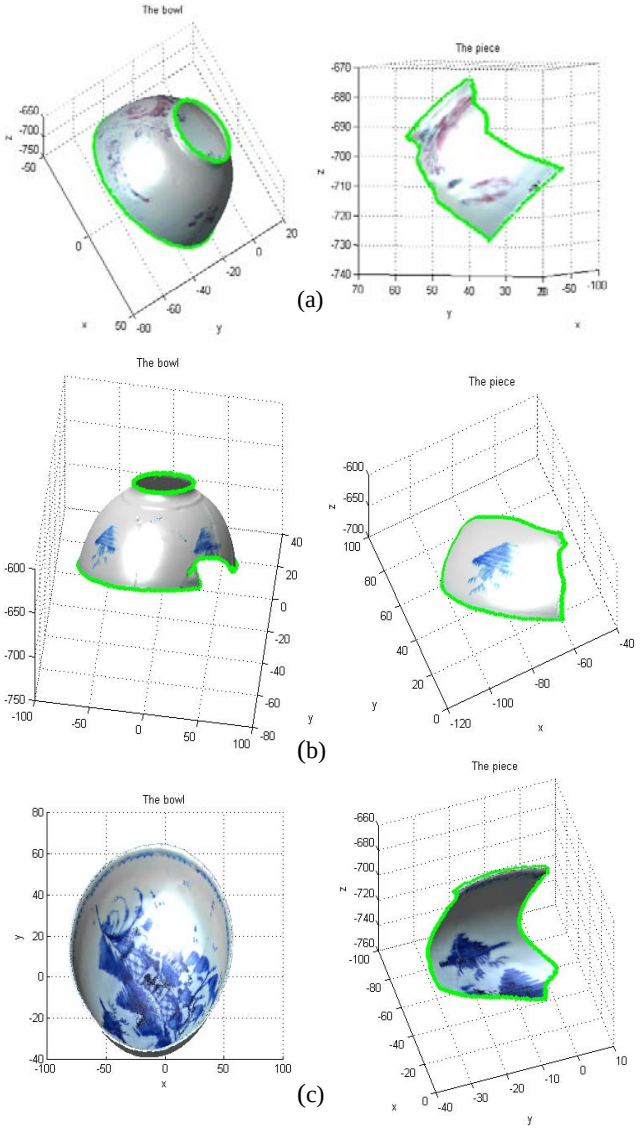

Figure 3: The 3D scans of the whole bowls and the pieces are given for (a) F191C105, (b) F193C112, and (c) F193C0122.

The contours on the surface are extracted using the texture information. The extracted contours are given in Figure 4 for the whole bowls and the pieces. The results of the alignments are shown in Figure 5. The detailed steps of the whole algorithm with the outputs at every step for the sample F191C105 are shown in Figure 6.

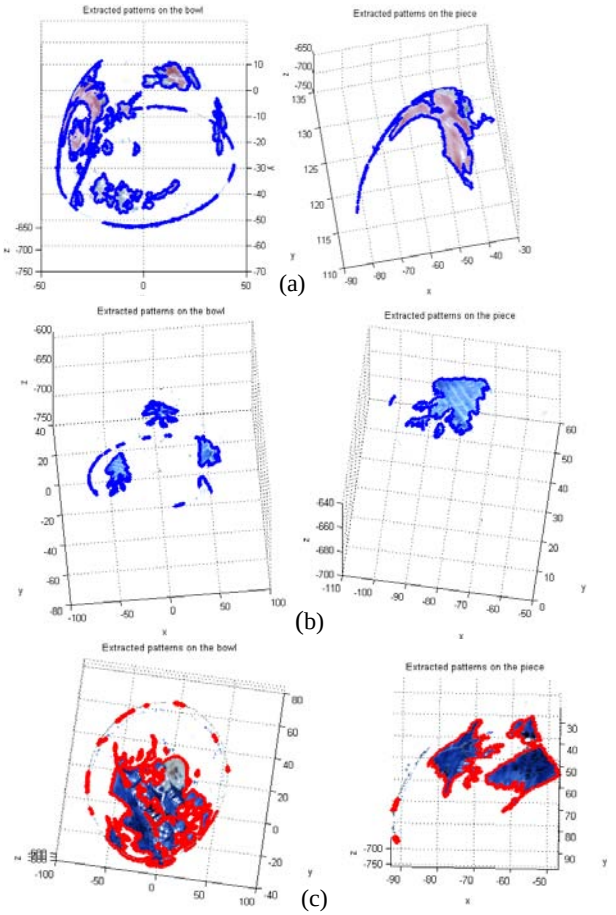

Figure 4: Extracted surface contours of (a) F191C105, (b) F193C112, and (c) F193C0122.

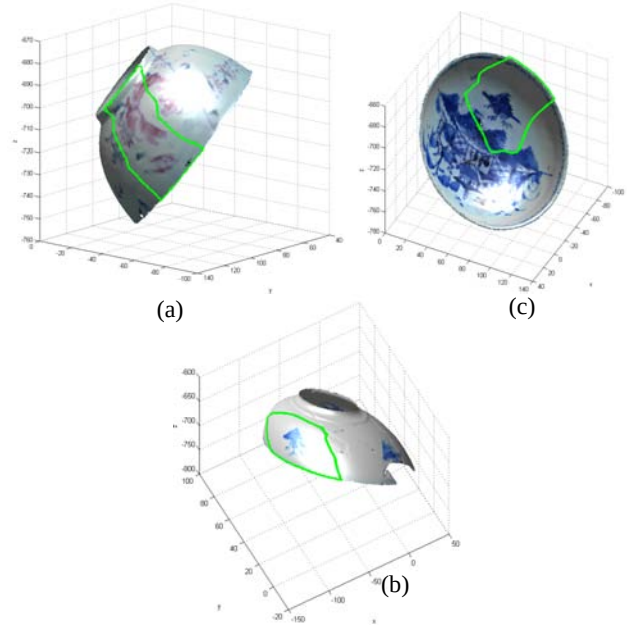

Figure 5: Alignment of the sample pieces on the original bowls for (a) F191C105, (b) F193C112, and (c) F193C0122.

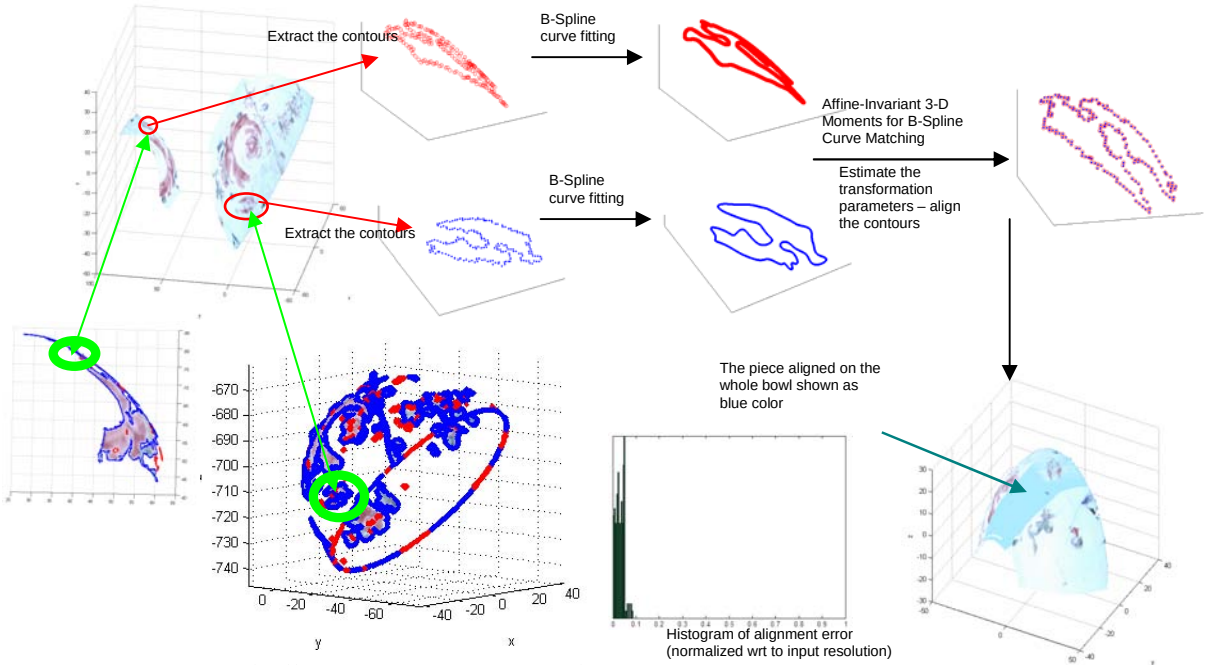

Figure 6. The detailed steps of Affine-Invariant 3-D Moments for B-Spline Curve Matching algorithm with the outputs given at every step.

5.3. Error Metric to evaluate the Accuracy of the Alignment

We define the residual error as the distance between two corresponding points for aligned surface pair (Surface 1 and Surface 2 – S1 and S2):

$$e_k = \min_{S1 \in Surface1} \|S2_k - S1\| \qquad (21)$$

In order to be able to analyze the amount of error for different surfaces on the same platform we normalize the error with respect to the mean resolution of S1. We define the resolution of Surface 1 as.

$$res_k = \min_{S1_l \in Surface1} \|S1_k - S1_l\| \quad , k \neq l \qquad (22)$$

The residual error statistics are given in Table 1.

Table 1: Error statistics for surface alignment using moments for the sample surface pairs.

Surface pair	Normalized Error $[\text{mean}(e_k) \pm \text{std}(e_k)]/\text{mean}(res_k)$
F191C105 outer surface	0.0865 ± 0.0493
F193C112 outer surface	0.0658 ± 0.0312
F193C0122 inner surface	0.0782 ± 0.0401

6. Intrinsic Fiducial Points/Curves on Vessel Surfaces in the absence of Marking Contours

For vessels that have no markings on their surfaces, in this case, the curves that we use for the alignment are computed from the intrinsic differential geometry of the surface and are also local affine preserved. One such curve sets are the parabolic curves introduced in [20]. These are connected curves points characterized by the vanishing of Gaussian curvature on them [20, 28-32]. They occur generically on curves called parabolic curves [28]. These curves are smooth loops that never intersect.

The parabolic points are the points where Gaussian curvature changes sign, combining them into parabolic contours are done by connecting them along the surface where hyperbolic regions change to elliptic regions. The parabolic contours are intrinsic and preserved under affine transformation making them very attractive for our purpose [33]. Note that unlike maximum and minimum curvature points, which are only preserved under the class of similarity transformations, parabolic contour points are preserved under similarity and affine transformations. The parabolic contour points can be used as fiducial points and used for alignment or can be grouped into parabolic contour curves. In this paper, we have elected to follow the latter as they are many parabolic contour points on the vessel. The 3D scans of the whole bowls and the pieces are given in Figure 7. The extracted parabolic contours are given in Figure 8. The result of the alignment using the corresponding parabolic curves is shown in Figure 9. The residual error statistics are given in Table 2.

Table 2: Error statistics for surface alignment using parabolic contours for the sample surface pairs.

Surface pair	Normalized Error $[\text{mean}(e_k) \pm \text{std}(e_k)]/\text{mean}(res_k)$

F142C074 outer surface	0.3619 ± 0.2478
F91C0120 outer surface	0.3706 ± 0.4480

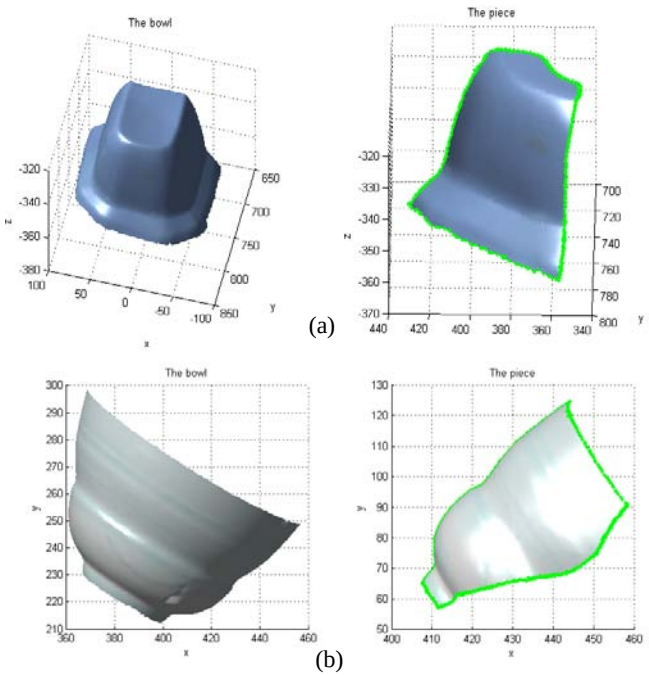

Figure 7: The 3D scans of the whole bowls and the pieces are given for (a) F142C074 and (b) F91C0120.

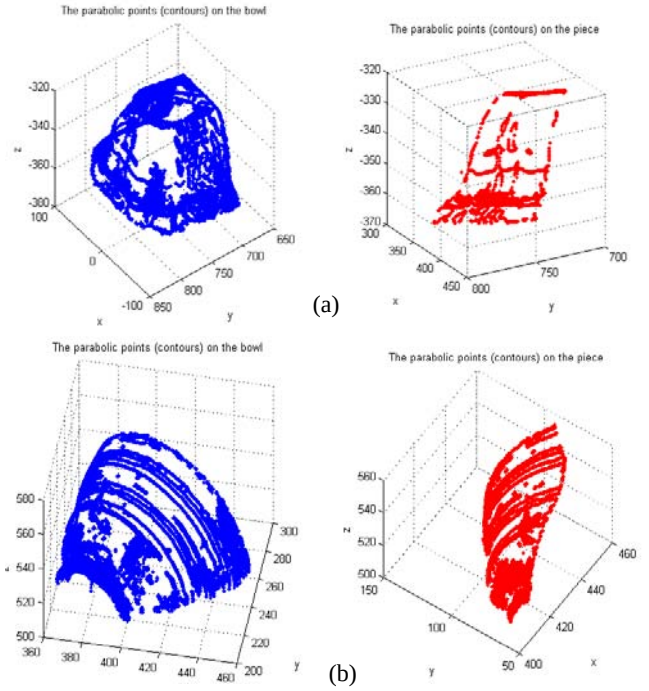

Figure 8: The extracted parabolic contours for (a) F142C074 and (b) F91C0120.

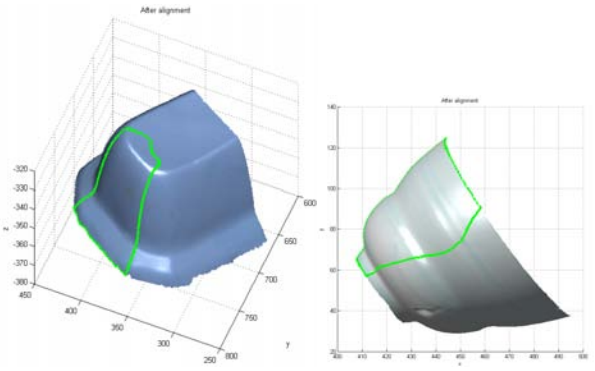

Figure 9: The result of the alignment using the corresponding parabolic curves for (a) F142C074 and (b) F91C0120.

7. Conclusions and Future Directions

We present two different methodologies to align the surfaces based on different aspects of the data, ranging from surface markings to surface intrinsic characteristics. These methods are illustrated using ceramic artifact collection recovered from the National Constitution Center site. We tested our first method using novel weighted moment invariants on three different vessels (F191C105, F193C112, and F193C0122), which have surface markings on them. The results are reported in terms of normalized residual error statistics, and the reported average errors are in the range of 0.066-0.087. The second method is tested on two different vessels (F142C074 and F91C0120) without textural information. The results are reported in terms of normalized residual error statistics, and the reported average errors are in the range of 0.3619-0.3706 which is still much lower than the resolution of the input. The selected methods are shown to be reliable on the sample set chosen from ceramic artifact collection recovered from the National Constitution Center site.

This research is part of a collaborative project for which the main objective is to develop novel computer vision research technology that can assist in the reconstruction of ceramic artifacts recovered from within an excavation context which, often times are fragmentary and with missing pieces. The whole project as an application of computer vision in archaeology will be unique as an enabling technology for timely analysis, interpretation, and presentation of this history evidence. It is also considered as great value and need by the U.S. Department of the Interior National Park Service.

Acknowledgements

This work is supported by the National Science Foundation, Division of Information & Intelligent Systems, under grant # 0803670 entitled “The 3D Colonial Philadelphia Project—Digital Restoration of Thin-Shell Objects for Historical Archaeological Research and Interpretation”. We would like to thank David Myers and

Girish Balakrishnan from Drexel University for their valuable help and efforts during the 3D scanning. We would also like to thank Patrice Jeppson from Drexel University for her valuable help and expertise in artifact selection and mending.

8. References

[1] S. Olsen, A. Brickman, and Y. Cai, "Discovery by Reconstruction: Exploring Digital Archeology," in *SIGCHI Workshop (Ambient Intelligence for Scientific Discovery (AISD))* Vienna, April 25, 2004.

[2] J. B. Benedict and R. Szymon, "Global non-rigid alignment of 3-D scans," in *ACM SIGGRAPH 2007 papers* San Diego, California: ACM, 2007.

[3] A. Karasik and U. Smilansky, "3D scanning technology as a standard archaeological tool for pottery analysis: practice and theory," *Journal of Archaeological Science*, vol. 35, pp. 1148-1168, May 2008.

[4] A. Bujakiewicz, M. Kowalczyk, P. Podlasiak, and D. Zawieska, "3D Reconstruction and Modelling of the Contact Surfaces for the Archaeological Small Museum Pieces," in *Proceedings of the ISPRS Commission V Symposium 'Image Engineering and Vision Metrology'*, Dresden, Germany, 25-27 September 2006.

[5] L. Van Gool and R. Sablatnig, "Special issue on 3D acquisition technology for cultural heritage," *Machine Vision and Applications*, vol. 17, pp. 347-348, Dec 2006.

[6] M. Kampel and R. Sablating, "3D data retrieval of archaeological pottery," *Interactive Technologies and Sociotechnical Systems*, vol. 4270, pp. 387-395, 2006.

[7] H. Mara, M. Kampel, F. Niccolucci, and R. Sablatnig, "Ancient coins & ceramics – 3D and 2D documentation for preservation and retrieval of lost heritage," in *Proceedings of the 2nd ISPRS International Workshop 3D-ARCH 2007: "3D Virtual Reconstruction and Visualization of Complex Architectures"*, ETH Zurich, Switzerland, July 12–13, 2007.

[8] A. Koutsoudis, G. Pavlidis, F. Arnaoutoglou, D. Tsiafakis, and C. Chamzas, "Qp: A tool for generating 3D models of ancient Greek pottery," *Journal of Cultural Heritage*, vol. 10, pp. 281-295, 2009/6// 2009.

[9] F. Kleber and R. Sablatnig, "A Survey of Techniques for Document and Archaeology Artefact Reconstruction," in *Document Analysis and Recognition, 2009. ICDAR '09. 10th International Conference on*, 2009, pp. 1061-1065.

[10] P. C. Igwe and G. K. Knopf, "3D Object Reconstruction Using Geometric Computing," in *Geometric Modeling and Imaging--New Trends, 2006*, 2006, pp. 9-14.

[11] G. Papaioannou and E. A. Karabassi, "On the automatic assemblage of arbitrary broken solid artefacts," *Image and Vision Computing*, vol. 21, pp. 401-412, May 1 2003.

[12] P. Stavrou, P. Mavridis, G. Papaioannou, G. Passalis, and T. Theoharis, "3D object repair using 2D algorithms," *Computational Science - Iccs 2006, Pt 2, Proceedings*, vol. 3992, pp. 271-278, 2006.

[13] J. C. McBride and B. B. Kimia, "Archaeological Fragment Reconstruction Using Curve-Matching," in *Computer Vision and Pattern Recognition Workshop, 2003. CVPRW '03. Conference on*, 2003, pp. 3-3.

[14] A. R. Willis and D. B. Cooper, "Bayesian assembly of 3D axially symmetric shapes from fragments," in *Computer Vision and Pattern Recognition, 2004. CVPR 2004. Proceedings of the 2004 IEEE Computer Society Conference on*, 2004, pp. I-82-I-89 Vol.1.

[15] M. Kampel and R. Sablatnig, "Virtual reconstruction of broken and unbroken pottery," in *3-D Digital Imaging and Modeling, 2003. 3DIM 2003. Proceedings. Fourth International Conference on*, 2003, pp. 318-325.

[16] G. Ucoluk and I. H. Toroslu, "Automatic reconstruction of broken 3-D surface objects," *Computers & Graphics-Uk*, vol. 23, pp. 573-582, Aug 1999.

[17] W. Rodriguez, M. Last, A. Kandel, and H. Bunke, "3-Dimensional curve similarity using string matching," *Robotics and Autonomous Systems*, vol. 49, pp. 165-172, 2004.

[18] Y. Lu, H. Gardner, H. Jin, N. Liu, R. Hawkins, and I. Farrington, "Interactive Reconstruction of Archaeological Fragments in a Collaborative Environment," in *Digital Image Computing Techniques and Applications, IEEE 9th Biennial Conference of the Australian Pattern Recognition Society on*, 2007, pp. 23-29.

[19] F. S. Cohen, W. Ibrahim, and C. Pintavirooj, "Ordering and parameterizing scattered 3D data for B-Spline surface approximation," *Ieee Transactions on Pattern Analysis and Machine Intelligence*, vol. 22, pp. 642-648, Jun 2000.

[20] F. S. Cohen and C. Pintavirooj, "Invariant surface alignment in the presence of affine and some nonlinear transformations," *Medical Image Analysis*, vol. 8, pp. 151-164, 2004.

[21] L. A. Piegl and W. Tiller, *The NURBS book*, 2nd ed. Berlin ; New York: Springer, 1997.

[22] P. L. Jeppson, "New Methods -- and forthcoming Records!... ," *http://diggininthearchives.blogspot.com*, 2009.

[23] http://www.nps.gov/inde/index.htm.

[24]http://www.konicaminolta.com/instruments/products/3d/non-contact/vivid910/index.html.

[25] http://www.geomagic.com/en/products/studio/index.shtml.

[26] C. De Boor, *A practical guide to splines*. New York: Springer-Verlag, 1978.

[27] Z. H. Huang and F. S. Cohen, "Affine-invariant B-Spline moments for curve matching," *Ieee Transactions on Image Processing*, vol. 5, pp. 1473-1480, Oct 1996.

[28] J. J. Koenderink and A. J. van Doorn, "Surface shape and curvature scales," *Image and Vision Computing*, vol. 10, pp. 557-564, 1992.

[29] W. Kühnel, *Differential geometry : curves - surfaces - manifolds*, 2nd ed. Providence, R.I.: American Mathematical Society, 2006.

[30] D. F. Rogers, "An introduction to NURBS with historical perspective," San Francisco: Morgan Kaufmann Publishers, 2001, pp. xvii, 324 p.

[31] E. V. Shikin and A. I. Plis, *Handbook on splines for the user*. Boca Raton: CRC Press, 1995.

[32] V. A. Toponogov and V. Y. Rovenskii, *Differential geometry of curves and surfaces : a concise guide*. Boston: Birkhäuser, 2006.

[33] J. L. Mundy and A. Zisserman, *Geometric invariance in computer vision*. Cambridge, Mass.: MIT Press, 1992.